Pure and Multicomponent Gas Diffusion within Zeolitic Adsorbents: Pulsed Field Gradient NMR Analysis and Model Development

Frank Rittig,† Charles G. Coe, and John M. Zielinski*

Air Products and Chemicals, Inc., 7201 Hamilton Boulevard, Allentown, Pennsylvania 18195

Received: August 22, 2002; In Final Form: December 27, 2002

The self-diffusion of gases within 5A- and 13X-type zeolites has been investigated using pulsed field gradient (PFG) NMR. Self-diffusion coefficients for pure carbon monoxide, methane, and nitrogen within commercially available zeolitic adsorbents have been measured as a function of pressure and temperature. In addition, we elucidate the effect of gas composition on transport rate by measuring diffusion of the corresponding binary and ternary gas mixtures within these zeolites. The diffusion process in both the pure and multicomponent systems is well-described by a long-range diffusion model (LRDM) that requires only adsorbent porosity and isotherm data. The general applicability of this model is critically evaluated by (1) analyzing pure gas self-diffusion within porous media as a function of pressure; (2) predicting self-diffusion coefficients while simultaneously varying pressure, temperature, and sorbate loading; and (3) extending these predictions to address diffusion in binary and ternary gas systems. The tortuosity factors derived from this study are reasonable, characteristic of the adsorbent, and gas-independent.

Introduction

The (self-) diffusion coefficient of a gas in microporous adsorbent materials is among the most important parameters describing mass transfer through adsorbent beds,[1] since diffusion rates often control cycle times and influence the design of industrial separation processes. Mass transfer through a commercial zeolitic material, which is typically produced by compressing a crystalline powder with a binder into a pellet, depends on both intra- and intercrystalline diffusion. In the absence of diffusion barriers, intercrystalline diffusion is responsible for the dominant mass transfer resistance in most commercial gas separation processes.[2] Molecular self-diffusion under isothermal conditions has been investigated in a wide variety of homogeneous systems, such as polymer solutions and melts,[3] as well as heterogeneous systems including gel electrolytes,[4] biological[5] and surfactant systems,[6] and porous solids.[1] In this work, we have applied pulsed field gradient (PFG) NMR to measure the self-diffusion coefficients of carbon monoxide, methane, and nitrogen in nanoporous media—commercial 5A and 13X zeolites—at pressures ranging from 0.5 to 5 atm.

The most applicable theory available to describe self-diffusion in nano/microporous crystalline powders has been proposed by Kärger et al.[7] The long-range diffusion model (LRDM) predicts self-diffusion in such systems reasonably well by assuming that the long-range self-diffusivity (D_i^{LR}) is governed predominantly by transport through intercrystalline space. Although developed in the early 1980s, this model has never been, to the best of our knowledge, critically evaluated. In addition to using PFG NMR to measure self-diffusion coefficients in zeolites, a second objective of the present work is to extend the LRDM to describe transport within pelletized zeolites and, subsequently, test its predictive accuracy and applicability. While the original model was developed for powders, the extended version is applied here to porous zeolitic pellets, which are of more practical relevance, by appropriately defining characteristic porosity values and considering simultaneous transport in both macro- and mesopores.[1,8,9] Although gas diffusion studies within zeolites continue to attract much attention, no satisfactory means of predicting multicomponent gas transport in zeolites as a function of temperature, pressure, and composition has ever been proposed.[1] We seek to address this shortcoming through our modified LRDM, as well as ascertain the explicit temperature dependence of gas diffusion in zeolites under variable surface excess conditions.

Experimental Section

Sample Preparation. The procedure to produce samples was previously described[8,10] and is only summarized here. Pelletized zeolites were obtained from UOP (Des Plaines, IL) and activated (to remove adsorbed water) under dynamic vacuum ($<10^{-4}$ Torr) and a 1 K/min thermal ramp. The pellets were held for 60 min at 373, 423, 473, and 523 K and ultimately heated for at least 12 h at 673 K. After activation, the samples were transferred without exposure to air to an Ar-purged glovebox, wherein a known amount of activated material was placed in a 10 mm quartz NMR tube. The sample tube was sealed using a valve and attached to a classical volumetric expansion unit (ASAP 2010 from Micromeritics, Inc., Norcross, GA). After degassing at ambient temperature to $<10^{-4}$ Torr, samples containing 0.5−5 atm ^{13}CO (99+%, Isotech), CH_4 (APCI), and/or $^{15}N_2$ (99+%, Isotech) were prepared.

Samples for analysis by PFG NMR were prepared as follows. The free space volume within a given NMR sample tube was determined by helium expansion. After evacuation, the calibrated manifold was charged to a particular pressure with the gas of interest. Upon equilibration, the gas was expanded into the sample cell and the sample tube was immediately immersed into liquid nitrogen. The tube was then sealed, and the free space lost as a result was determined from a second He expansion

* To whom correspondence should be addressed.
† Present address: BASF AG, GKP/P-G200, D-67056 Ludwigshafen, Germany.

10.1021/jp0219451 CCC: $25.00
Published on Web 04/16/2003

test. The resulting cell volume was determined by difference. Although the pressure within the NMR sample tube and the surface excess on the zeolite could be calculated from knowledge of an isotherm (measured independently) and an appropriate equation of state for the gas phase, gas-phase NMR was typically performed[10] to obtain direct measurements of these parameters. In multicomponent gas systems, gas-phase NMR analysis was critical, since multicomponent equilibria data were unavailable for our systems.

The porosities and associated pore size distributions of the zeolites were determined by complementary mercury intrusion, helium pycnometry, and N_2 isotherm measurements performed at 77 K. The mean pore diameter employed in our self-diffusion analyses was the hydraulic (or tubular) diameter.[11]

PFG NMR Analysis. The NMR data were collected using a Bruker AMX-360 NMR spectrometer equipped with a wide-bore magnet, which has been described earlier.[8] The instrument was outfitted with a Bruker microimaging accessory that includes the gradient pulse amplifiers required to generate field gradients. The NMR probe was equipped with either a $^{15}N/^{1}H$ or a $^{13}C/^{1}H$ double-tuned radio frequency coil insert, which can accommodate sample tubes measuring up to 10 mm in diameter. The specimen temperature was maintained to within an accuracy of ± 0.5 K using a Eurotherm B-VT2000 temperature control unit. For diffusion measurements, the stimulated echo sequence ($\pi/2-\tau-\pi/2-t'-\pi/2-\tau-$fid) was used because the spin−spin-relaxation times (T_2) are usually much shorter than the spin−lattice relaxation times (T_1).[12] All experiments were performed to ensure that the self-diffusion coefficients being measured were time-independent. The experiments were performed by increasing the gradient strength incrementally while maintaining the diffusion times (t' and τ) constant. Typical values for $t' + \tau$ ranged between 21 and 52 ms. The maximum gradient strength was127 G/cm.[8]

In the case of a random walk, the measured spin attenuation, Ψ, due to the field gradient applied after the first and third $\pi/2$ rf pulses, can be described by the application of a Gaussian propagator, namely,[2]

$$\Psi = \frac{A}{A_0} = \exp(-q^2 D\Delta) \tag{1}$$

where $2D\Delta$ represents the mean square displacement of the diffusing molecules, D is the experimental self-diffusion coefficient, and Δ is the diffusion time ($\Delta = t' + \tau$). The parameter q represents the product $\delta\gamma g$, where δ is the duration of the gradient pulse, g is the strength of the gradient pulses, and γ is the gyromagnetic ratio of the nucleus of interest (e.g., ^{1}H, ^{13}C, or ^{15}N). Equation 1 is valid only in the narrow pulse approximation[2] ($\Delta \gg \delta$) which was strictly considered in our experiments. The total magnetization amplitudes with and without applied gradients are A and A_0, respectively. No additional gradient adjustment is necessary when two pregradients are applied prior to the pulse sequence with the same gradient strength and duration. In all of the experiments performed, the mean square displacement was at least an order of magnitude (generally two) greater than the size of a zeolite crystal. Consequently, the self-diffusion coefficients measured were long-range coefficients and not intracrystalline diffusion coefficients. The size of the zeolite crystal is $\sim 1\ \mu$m while the rms distance traveled was $> 30\ \mu$m.

Besides ^{1}H and ^{19}F PFG NMR, relatively few experiments using ^{15}N and ^{13}C nuclei have been reported.[8,13,14] To independently ascertain the consistency of our experimental methods, ^{1}H and ^{13}C PFG NMR experiments were performed using 99% ^{13}C-labeled CH_4, thereby facilitating analysis of the diffusion process through either the ^{1}H or ^{13}C nuclei of the methane molecule. The echo attenuations and resulting diffusion coefficients obtained from both analyses were identical.

Results and Discussion

Model Considerations. We begin by revisiting the theory developed by Kärger et al.[7] for describing the long-range self-diffusion behavior of gases within microporous particles. The LRDM captures the fundamental physics that permit reasonable prediction of gas self-diffusion within microporous crystalline powders. It assumes that transport through intercrystalline space regulates the long-range self-diffusivity (D_i^{LR}), the value of which for a diffusant within a microporous adsorbent medium can be approximated by

$$D_i^{LR} \cong p_i^{inter} D_i^{inter} \tag{2}$$

Here, p_i^{inter} is the mole fraction of molecules of species i within the pore space and D_i^{inter} is the corresponding self-diffusivity. The value of p_i^{inter} can be derived from the dynamic equilibrium between molecules residing in the inter- and intracrystalline space, viz.,

$$p_i^{inter} = \frac{\tau_i^{inter}}{\tau_i^{inter} + \tau_i^{intra}} \tag{3}$$

where τ_i^{inter} is the residence time of species i within in the pore region and τ_i^{intra} is the corresponding lifetime of the molecule within the zeolitic crystals. In all of the experiments performed in this work, there was fast exchange between the molecules in the intercrystalline pore space and the intracrystalline regions with no visible diffusion barriers. Consequently, all of the self-diffusion coefficients measured were time-independent and the echo decay curves were single-exponential.

To extend the LRDM for use with adsorbent pellets in which the molecular displacement measured by PFG NMR is much larger than a zeolite crystal and much smaller than the pellet size, the value of p_i^{inter} can be calculated directly from the adsorption isotherm of species i in conjunction with the characteristic dimensions of the particle:

$$p_i^{inter} = \frac{n_i^{inter}}{n_i^{inter} + n_i^{intra}} = \frac{c_i \epsilon_{ma}}{c_i \epsilon_{ma} + \rho_p n_i^{m}} = \frac{1}{1 + \dfrac{RT\rho_p n_i^{m}}{P_i \epsilon_{ma}}} \tag{4}$$

Here n_i^{inter} represents the total mole number of species i in the pore region, n_i^{intra} is the mole number of i adsorbed on the zeolite, c_i is the gas-phase concentration of i (in mol/cm^3 pore), n_i^{m} is the surface excess of i (in mol/g), ϵ_{ma} is the porosity, ρ_p is the particle density (in g/cm^3), P_i is the partial pressure of i, R is the gas constant, and T denotes absolute temperature. The ratio n_i^{m}/P_i represents the local chord to the sorption isotherm, which, in the limit of sufficiently low pressure, is equal to the Henry's constant.

The value of D_i^{inter} can be estimated using the kinetic theory of gases,[15] which yields

$$D_i^{inter} = \frac{1}{3}\sqrt{\frac{8RT}{\pi M}}\lambda_i^{inter} \tag{5}$$

where M is the molecular weight of the diffusant and the quantity within the square root yields the mean molecular

velocity of species *i*. The value of λ_i^{inter}, the effective molecular mean-free path of *i*, in pure and multicomponent gas mixtures can be calculated from[15]

$$\frac{1}{\lambda_i^{\text{inter}}} = \frac{1}{d_{\text{ma}}} + \sum_{j=1}^{n} \frac{1}{\lambda_{i-j}} \tag{6}$$

where d_{ma} identifies the effective pore diameter of the pore structure, λ_{i-i} is the collision distance between like molecules, and λ_{i-j} represents the collision distance between different molecules. Values of λ_{i-j} are given by

$$\lambda_{i-j} = \frac{RT}{\pi\sqrt{2}} \sum_{j=1}^{n} \frac{1}{P_j \left[\frac{\sigma_i + \sigma_j}{2}\right]^2} \tag{7}$$

where σ_i is the kinetic diameter of diffusant *i* and P_j is the corresponding partial pressure. In the present extension, the value of σ_i is taken to be the kinetic diameter of a molecule estimated from the minimum cross-sectional diameter in its Lennard-Jones potential.[16] The values adopted for σ_i for CO, N_2, and CH_4 are 3.76, 3.64, and 3.8 Å, respectively. The effective pore diameter, d_{ma}, is taken as the tubular or hydraulic diameter ($d_{\text{ma}} = 4V_{\text{cum}}/A_{\text{cum}}$, where V_{cum} and A_{cum} are the cumulative pore volume and area, respectively) from Hg porosimetry. The value of d_{ma} must be determined carefully, since it strongly influences the predicted pressure dependence of long-range diffusivity (i.e., it determines the relative placement of the Knudsen diffusion and Henrian sorption limits, as discussed later).

Combination of eqs 2−7 reveals that predictions for D_i^{LR} rely exclusively on porosity and isotherm data. These predictions are, however, founded on the assumption that mass transport occurs only in idealized cylindrical pores, which is consistent with other diffusion models (e.g., the dusty gas model[17]). Although the general trends of these predictions are expected to follow experimental data well, experimental diffusion coefficients are expected to be smaller in magnitude due to tortuosity.[17] Tortuosity factors can be deduced by comparing theoretical predictions of self-diffusion in porous media to self-diffusion coefficients measured from experiments such as PFG NMR. In the next section, we assess the predictive efficacy of the LRDM by comparing predicted and experimental self-diffusion coefficients.

Pure Gas Diffusion within Zeolites. The self-diffusion coefficients of pure CO, CH_4, and N_2 have been measured as a function of pressure within a series of 5A and 13X pelletized materials. The pressure dependence for all these gases is described well by the LRDM (eq 2), as seen in Figure 1. The lines in this figure represent fits of the LRDM in which the tortuosity is considered an adjustable parameter. The porosity parameters extracted from these correlations are listed in Table 1 and are, within experimental uncertainty, independent of gas but dependent on adsorbent. This result is entirely consistent with the expectation that tortuosity represents a physical characteristic relating to the structure of an adsorbent, and not an arbitrary constant. The average tortuosity values determined here are reasonable in light of independent measurements reported for the adsorbents investigated here. As a side note, a better correlation of the experimental data is obtained by simultaneously adjusting both the tortuosity and effective pore diameter. If a single value of d_{ma} is used, it must be measured as accurately as possible, especially if accurate diffusion

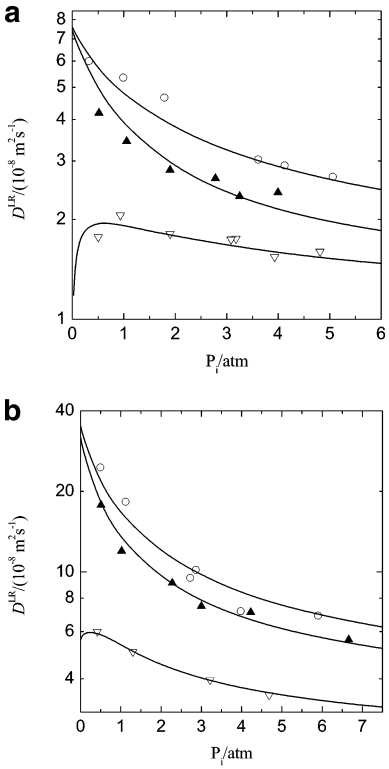

Figure 1. Long-range self-diffusion coefficients of CO (△), CH_4 (▲), and N_2 (○) as a function of pressure for pure gases on (a) 5A-I and (b) 13X zeolite. The lines represent regressed fits of the diffusion data using the LRDM with constant tortuosity factors of 2.8 and 1.5 for the 5A-I and 13X zeolite, respectively.

TABLE 1: Parameters Used in LRDM Predictions for 5A-I, 5A-II, and 13X Zeolites

parameter	5A-I	5A-II	13X
d_{ma}/Å	998	1300	1667
ϵ_{ma}	0.288	0.315	0.293
ρ_{P}/(g cm^{-3})	2.54	2.52	2.42

predictions are required at low pressures. We will return to this point shortly.

The diffusion data in Figure 1 clearly show that the most strongly adsorbed gas (CO) exhibits the lowest (long-range) diffusivity, whereas the weakest adsorbed gas (N_2) possesses the fastest long-range mobility. A more highly energetic gas−solid interaction tends to favor a lower population of gas molecules in the intercrystalline space and, therefore, a lower value of p_i^{inter} and, ultimately, D_i^{LR}. The maximum in the long-range diffusion coefficients of CO as a function of increasing pressure is somewhat surprising. One intuitively expects that the number of collisions a gas molecule experiences would increase monotonically with increasing pressure, thereby yielding smaller diffusion coefficients. Conversely, D_i^{inter} is anticipated to increase with decreasing pressure. This expectation is observed in Figure 1 at pressures above ~1 atm. In contrast, as the pressure is reduced further, D_i^{inter} remains constant as the Knudsen limit is reached. The maximum evident in $D_i^{\text{LR}}(P_i)$ reflects the fact that D_i^{LR} is affected by the pressure dependence not only of D_i^{inter} but also of p_i^{inter}. Recall that, at low pressure, n_i^{m} is directly proportional to P_i (in the Henry's law regime) and, according to eq 4, p_i^{inter} should be independent of pressure. Outside the Henrian limit, the ratio n_i^{m}/P_i is less than the Henry's constant for a type I isotherm, in which case p_i^{inter} increases with increasing pressure. This point is illustrated in Figure 2. The opposing dependences of D_i^{inter} and p_i^{inter} with

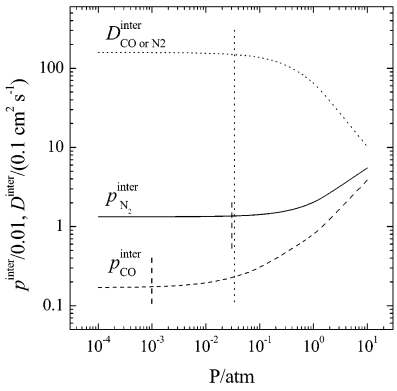

Figure 2. Pressure dependence of D_i^{inter} (•••), p_i^{inter} for pure CO (- - -), and p_i^{inter} for pure N_2 (—) calculated for the 5A-I zeolite. The vertical lines indicate the transition pressures for Knudsen diffusion and Henrian adsorption.

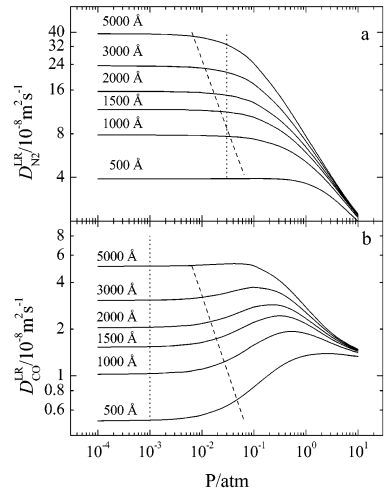

Figure 3. Influence of the pore diameter on the pressure dependence of (a) N_2 and (b) CO long-range diffusion within the 5A-I zeolite predicted by the LRDM. Included in the graph are lines identifying the transition into the Henrian adsorption (dotted) and Knudsen diffusion (dashed) regimes.

increasing pressure are, therefore, together responsible for the apparent maximum in $D_i^{LR}(P_i)$.

As stated earlier, besides the sorption isotherm, the tubular diameter (d_{ma}) constitutes the most sensitive physical parameter within the context of the LRDM. To illustrate the importance of this parameter (especially at low pressure), curves representing D_{CO}^{LR} and $D_{N_2}^{LR}$ as functions of pressure have been generated for different effective diameters over a typical range of 500−5000 Å. These results, generated with all other parameters held constant, are presented for comparison in Figure 3. The porosity and isotherm parameters used in these calculations are for the 5A-I zeolite (see Table 1). Two features of Figure 3 are particularly noteworthy. The first, designated by a dotted line, is the pressure below which Henry's law describes equilibrium, that is, p_i^{inter} is constant. The second feature (signified by the dashed line) identifies when the Knudsen limit is reached and D_i^{inter} is equal to the Knudsen diffusion coefficient.[18] Variation in d_{ma} is observed to affect not only the magnitude of D_i^{inter} (especially at low pressure) but also the nature of the system in terms of its thermodynamic or transport characteristics.

For a fixed value of d_{ma}, the shape of the $D^{LR}(P)$ curve is dictated predominantly by the relative positions of the Knudsen and Henry's law regimes. As the pressure is reduced to ∼1 atm, the long-range diffusivity increases due to the decreasing number

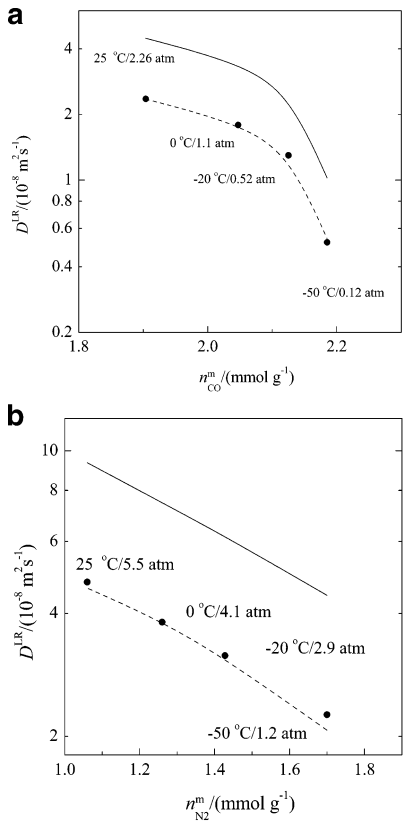

Figure 4. Long-range self-diffusion coefficients for (a) CO and (b) N_2 within 5A-II as a function of surface excess (capacity). The solid lines are predictions from the LRDM with no adjustable parameters (unity tortuosity factor), while the dotted lines denote the same predictions reduced by a constant tortuosity factor of 2.0, determined from pure gas diffusion studies of CO and N_2 within 5A-II.

of gas−gas collisions, even though p_i^{inter} continuously decreases over the same pressure range. A further decrease in pressure yields an increased contribution of gas−wall collisions to the molecular mean-free path and a corresponding increase in the intrinsic molecular mobility. This increase in diffusion rate is evident until the Knudsen limit is reached, wherein the intercrystalline diffusion coefficient attains a limiting value. As d_{ma} becomes smaller, the transition into the Knudsen regime occurs at higher pressures, resulting in a continuous increase in the long-range diffusivity up to the Henrian limit. For nitrogen, the most weakly adsorbed gas examined here, the Henrian limit exists at pressures below 0.03 atm at 25 °C.

Another consideration of importance in the present work is the temperature dependence of self-diffusion coefficients. Since the tortuosity factor is presumed to be a physical characteristic associated with the structure of a given porous solid, it immediately follows that tortuosity factors should be independent of temperature and adsorbate. To test this hypothesis, PFG NMR analysis of CO and N_2, the most strongly and weakly adsorbed gases, respectively, examined in this study, has been performed to deduce D^{LR} in zeolite 5A-II at select temperatures between −50 and 25 °C (see Figure 4). Since the system under investigation is closed, a change in sample temperature is accompanied by a redistribution of molecules between the gas phase and the solid surface as the system seeks to re-establish equilibrium. Consequently, the pressure *and* loading vary simultaneously as temperature is varied. In Figure 4, we compare experimental PFG NMR data with predictions from the LRDM using tortuosity values of 1 (solid line) and 2 (dotted line). A tortuosity of 1 physically represents an idealized structure in which transport proceeds within a straight cylindrical pore, while

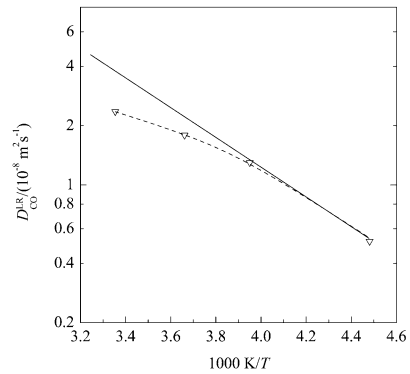

Figure 5. Long-range diffusion coefficients for CO (▽) within 5A-I zeolite as a function of reciprocal absolute temperature. The solid line is a fit of the Arrhenius equation to the two data points measured at the lowest temperatures, and the dashed line is predicted from the LRDM.

a value of 2 has been extracted from the pressure dependence of D^{LR} for pure CO and N_2 in 5A-II. The LRDM predictions are in excellent agreement with the experimental data, which, along with the reasonable and adsorbate-independent value of the tortuosity factor, is consistent with the presumption that tortuosity constitutes an adsorbent-specific structural property.

An unexpected result is that the experimental values of D_i^{LR} do not exhibit Arrhenius behavior with respect to temperature, as illustrated in Figure 5. Included in this figure is the corresponding prediction from the LRDM, which agrees well with the data at low temperatures. Since the activation energy of diffusion changes appreciably over this temperature range, it does not equate to the heat of adsorption, as is often assumed. Even if the experimental data had exhibited Arrhenius behavior, it is not generally appropriate to assess them in the context of this relationship because the experimental conditions are not isosteric. In general, the activation energy obtained from such analysis should not be compared with the isosteric heat of adsorption. This shortcoming can be overcome if one considers the temperature dependence of D_i^{LR} as $p_i \rightarrow 0$. In this limiting case, the temperature dependence of D_i^{inter} can be accurately described in terms of the Knudsen diffusivity ($D_i^{inter} \propto \sqrt{T}$), and adsorption equilibrium is given by Henry's law so that eq 4 becomes

$$\lim_{p\to 0} p_i^{inter} = \frac{1}{1 + \dfrac{RT\rho_p K_H}{\epsilon_{ma}}} \tag{8}$$

If the Henry's constant ($K_H \propto \exp(-q_{iso}/RT)$) exhibits Arrhenius behavior with q_{iso} taken as the isosteric heat of adsorption, the temperature dependences of p_i^{inter} and D_i^{LR} are given by, respectively

$$\lim_{p\to 0} p_i^{inter} \propto T^{-1} \exp\left(\frac{q_{iso}}{RT}\right)$$

and

$$\lim_{p\to 0} D_i^{LR} \propto \frac{\exp\left(\dfrac{q_{iso}}{RT}\right)}{\sqrt{T}} \tag{9}$$

Under the restrictions imposed, the activation energy for diffusion approximates the isosteric heat of adsorption.

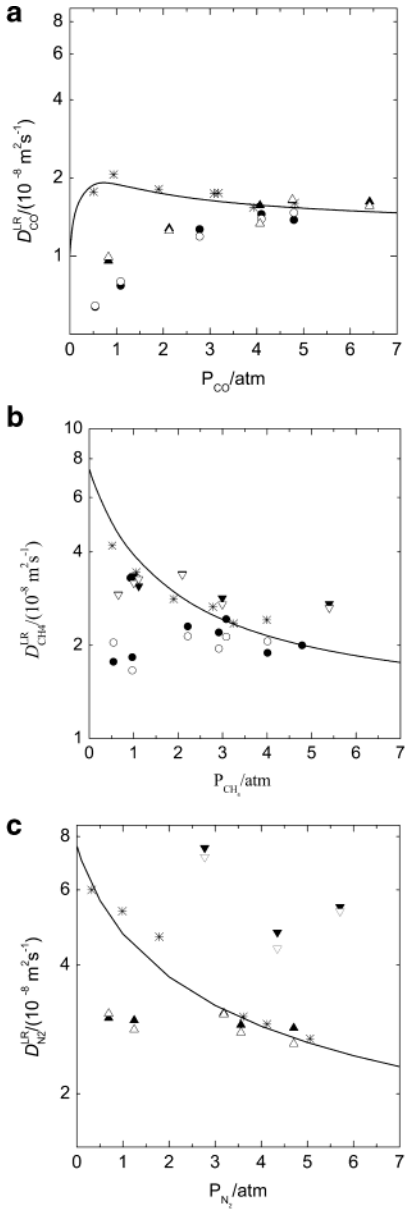

Figure 6. Long-range self-diffusion coefficients of (a) CO, (b) CH_4, and (c) N_2 in mixed gas systems as a function of pressure in the presence of CO (▼), CH_4 (▲), and N_2 (●) on 5A-I zeolite. In each figure the symbol ∗ represents the long-range diffusion coefficients for the corresponding pure-component system, and the solid line in each figure is the correlation of these data with the LRDM using constant tortuosity factors of 2.6, 3.0, and 2.7 for CO, CH_4, and N_2, respectively. The filled symbols represent experimental PFG NMR data, while the open symbols correspond to predictions from the LRDM using the tortuosity factors determined from pure gas adsorption.

Mixed Gas Diffusion within Zeolites. Next, we turn our attention to the diffusion of multicomponent gas mixtures within porous media by focusing on the diffusion of binary mixtures of CO, CH_4, and N_2 within the 5A-I zeolite. Included for comparison in Figure 6 are predictions from the LRDM for the pure gas (solid line) and binary mixtures (discrete points). These predictions use the tortuosity factors derived from the pure gas studies (see Figure 1a). The filled symbols represent PFG NMR data for specified binary systems, whereas the open symbols correspond to predictions from the LRDM for the gas of interest in the presence of either CO, CH_4, or N_2. In all cases, the samples analyzed have been prepared so that the total pressure within the sample tubes remained nearly constant (∼5 atm) at ambient temperature. The comparative analysis in Figure 6

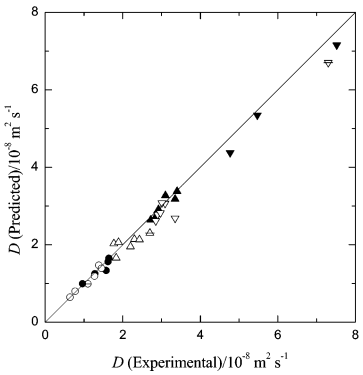

Figure 7. Parity plot of the experimental and predicted self-diffusion coefficients for CO in the presence of CH_4 (●), CO in the presence of N_2 (⊖), CO in the presence of CH_4 and N_2 (○); CH_4 in the presence of CO (▲), CH_4 in the presence of N_2 (◬), CH_4 in the presence of CO and N_2 (△); N_2 in the presence of CO (▼), N_2 in the presence of CH_4 (▽), and N_2 in the presence of CO and CH_4 (▽̲).

reveals very good quantitative agreement between the model predictions and the experimental data. Accurate prediction of gas mixture diffusion behavior requires accurate quantitation of the gas-phase pressure and the surface excess within the samples, which is achieved by NMR spectroscopy, as described in detail elsewhere.[10] In essence, the NMR signal intensity obtained from the gas phase above the adsorbent is correlated with pressure. From He free-space measurements, the number of moles residing in the gas phase can be calculated. Since the moles of adsorbate delivered into the sample tube and the mass of the adsorbent are also known, the surface excess of any NMR-active species can be directly ascertained. This method of measuring sorption equilibrium has been verified by comparing the results with those from classical volumetric and gravimetric experiments.

Figure 6a illustrates the diffusivity of CO in the presence of a second gas (CH_4 or N_2). At CO partial pressures lower than the system pressure, the diffusivity of CO in the mixture is lower than that in the pure gas at the same partial pressure. This trend is consistent with intuition, since additional molecular collisions occur when the system pressure is higher (∼5 atm) than the CO partial pressure due to the presence of a second gas. At CO partial pressures near the system pressure (in gas mixtures approaching the limit of pure CO), the diffusivity of CO correctly approaches that of the pure gas. It is reassuring that these expected and measured variations in diffusion coefficient are accurately captured by the LRDM. Similar behavior is generally observed for the diffusion of CH_4 in the presence of N_2 (Figure 6b) or N_2 in the presence of CH_4 (Figure 6c). In marked contrast, the diffusion coefficients for N_2 in the presence of CO (see Figures 6c) can be substantially *higher* than those for the pure gas at the same partial pressure below the system pressure! Such enhanced transport is an exclusive consequence of stronger CO adsorption on the adsorbent. Since CO molecules adsorb more strongly than N_2 molecules, they occupy a larger fraction of the adsorption sites. Consequently, more N_2 molecules are forced into the pores, since they are displaced from the solid, thereby promoting an increase in D^{LR}. As is evident in Figure 6, the LRDM accurately predicts this important effect. To emphasize the accuracy of the LRDM predictions, the data displayed in Figure 6 are provided as a parity graph in Figure 7, which clearly reveals the excellent predictive capability of the LRDM.

Last, we have investigated the diffusion of a ternary gas mixture within the 5A-I adsorbent.[9] As in the previous binary gas mixtures, the gas-phase NMR technique has been applied to measure the surface excess of the ternary gas mixture. Experimental results are seen in Table 2 to compare favorably with predictions from the LRDM. For further comparison, the diffusion coefficients of the pure gases within the zeolite at the corresponding partial pressure of each gas are experimentally determined and predicted to be 2 to 3 times greater than those in the ternary mixture. This result clearly reveals that the interplay between adsorption equilibria and molecular collisions within a multicomponent system significantly impacts overall mass transfer rates.

TABLE 2: Long-Range Self-Diffusion Coefficients ($\times 10^8$ m^2 s^{-1}) for a Ternary Gas Mixture within the 5A-I Adsorbent[a]

	D(CO)	D(CH_4)	D(N_2)
exp	1.1	2.7	7.3
pred	0.99	2.3	6.7

[a] The gas partial pressures were 2.8, 2.2, and 2.4 atm for CO, CH_4, and N_2, respectively, and the respective loadings were 1.4, 0.48, and 0.14 mmol g^{-1}. Predictions were made using the LRDM with use of the tortuosity factors determined from pure adsorbate/adsorbent systems.

Summary

We have demonstrated that the long-range diffusivity within zeolitic adsorbents can be accurately described by the long-range diffusion model initially proposed by Kärger et al.[7] for crystalline powders and extended here to describe gas diffusion in adsorbent pellets. Comparison of model predictions with experimental data acquired by PFG NMR yields tortuosity factors that can be used to accurately predict self-diffusion within multicomponent gas mixtures. The tortuosity factors determined in this fashion are reasonable in magnitude; independent of temperature, pressure, and adsorbate; and characteristic of the adsorbent. Additional experimental investigations show that the LRDM accurately predicts self-diffusion behavior under the most stringent conditions when pressure, temperature, and sorbate loading vary simultaneously. The transition pressures identifying the Knudsen diffusion regime and the Henrian adsorption limit, along with the value of the tubular diameter, are shown to be principally responsible for governing the pressure dependence of the long-range diffusion coefficient. Molecular diffusion rates of binary and ternary gas mixtures within 5A and 13X zeolites have been measured by PFG NMR. Although the long-range self-diffusion coefficient of a given gas is generally reduced due to the presence of additional diffusing species, the long-range diffusion coefficient of N_2 in binary mixtures of N_2 and CO is found to increase dramatically relative to that of pure N_2 at the same partial pressure. This abrupt increase, accurately predicted by the LRDM, is attributed to selective adsorption of CO on the surface of the adsorbent.

Acknowledgment. F.R. gratefully acknowledges financial support from the Alexander von Humboldt Foundation for this project. We also thank Prof. J. Kärger and Dr. S. Sircar for insightful discussions.

Nomenclature

A = total magnetization with applied gradient
A_0 = total magnetization without applied gradient
A_{cum} = cumulative pore area
c_i = gas-phase concentration of component I
d_{ma} = the effective pore diameter of the pore structure
D_i^{LR} = long-range self-diffusivity of component i
D_i^{inter} = diffusivity of species i in the intercrystalline pore region

g = strength of the gradient pulses
K_H = Henry's constant
M = molecular weight of the diffusing species
n_i^{inter} = mole number of species i in the pore region
n_i^{intra} = number of adsorbed moles of species i
n_i^{m} = surface excess of species i
P = total pressure
P_i = partial pressure of species i
p_i^{inter} = probability of species i in the pore region
q = abbreviation for $q = \delta\gamma g$
q_{iso} = isosteric heat of adsorption
R = universal gas constant
T = absolute temperature
t' = second time delay in the stimulated echo PFG sequence
T_1 = spin−lattice relaxation time
T_2 = spin−spin relaxation time
V_{cum} = cumulative pore volume
$\langle 2D\Delta \rangle$ = mean square displacement

Greek Letters

γ = gyromagnetic ratio of the investigated nucleus
δ = duration of the gradient pulse
Δ = diffusion time ($\Delta = t' + \tau$)
ϵ_{ma} = porosity
λ_{i-i} = collision distance between like molecules
λ_{i-j} = collision distance between unlike molecules
λ_i^{inter} = effective molecular mean-free path
π = rf pulse
ρ_p = particle density
τ = first time delay in the stimulated echo PFG sequence
τ_i^{inter} = residence time of species i in the pore region
τ_i^{intra} = residence time of species i in the zeolite
Ψ = measured spin attenuation

References and Notes

(1) Kärger, J.; Ruthven, D. M. *Diffusion in Zeolites and Other Microporous Solids*; John Wiley & Sons: New York, 1992.

(2) Kärger, J.; Pfeifer, H.; Heink, W. *Adv. Magn. Reson.* **1998**, *12*, 1. Kärger, J.; Fleischer, G.; Roland, U. In *Diffusion in Condensed Matter*; Kärger, J., Heitjans, P., Haberlandt, R., Eds.; Friedr. Vieweg & Sohn: Verlagsgesellschaft mbH, Braunschweig, 1998.

(3) Rittig, F.; Kärger, J.; Papadakis, C. M.; Fleischer, G.; Stepanek, P.; Almdal, K. *Phys. Chem. Chem. Phys.* **1999**, *1*, 3923. Anastasiadis, S. H.; Rittig, F.; Chrissopoulou; Fleischer, G.; Fytas, G.; Semenov, A. N.; Kärger, J.; Xenidou, M.; Pispas, S. E*urophys. Lett*. **2000**, *51* (1), 68.

(4) Bamford, D.; Dlubek, G.; Reiche, A.; Alam, M. A.; Meyer, W.; Galvosas, P.; Rittig, F. *J. Chem. Phys.* **2001**, *115*, 7260.

(5) Knauss, R.; Schiller, J.; Fleischer, G.; Kärger, J.; Arnold, K. *Magn. Reson. Med*. **1999**, *41*, 285.

(6) Söderman, O.; Stilbs, P. *Prog. Nucl. Magn. Reson. Spectrosc*. **1994**, *26*, 445.

(7) Kärger, J.; Kocirik, M.; Zikanova, A. *J. Colloid Interface Sci.* **1981**, *84* (1), 240.

(8) McDaniel, P. L.; Coe, C. G.; Kärger, J.; Moyer, J. D. *J. Phys. Chem.* **1996**, *100*, 16263.

(9) Rittig, F.; Coe, C. G.; Zielinski, J. M. *J. Am. Chem. Soc.* **2002**, *124* (19), 5264−5265.

(10) Rittig, F.; Aurentz, D. J.; Coe, C. G.; Kitzhoffer, R.; Zielinski, J. M. *Ind. Eng. Chem. Res.* **2002**, *41*, 4430−4434.

(11) *Analytical Methods in Fine Particle Technology*; Micromeritics Instrument Corporation: Norcross, GA, 1997; p 186.

(12) See, for example: Callaghan, P. T. *Principles of Magnetic Resonance Microscopy*; Clarendon Press: Oxford, 1993.

(13) Bär, N.-K.; McDaniel, P. L.; Coe, C. G.; Seiffert, G.; Kärger, J. *Zeolites* **1997**, *18*, 71.

(14) Stallmach, F.; Kärger, J.; Pfeifer, H. *J. Magn. Reson. A* **1993**, *102*, 270.

(15) Kärger, J.; Zikanova, A.; Kocirik, M. *Z. Phys. Chem. Leipzig* **1984**, *265*, 587.

(16) Breck, D. W. *Zeolites Molecular Sieves*; John Wiley & Sons: New York, 1974; p 634.

(17) Evans, R. B.; Watson, G. M.; Mason, E. A. *J. Chem. Phys.* **1961**, *35* (6), 2076.

(18) Satterfield, C. N. *Mass Transfer in Heterogeneous Catalysis*; MIT Press: Cambridge, MA.